A MULTISCALE STUDY OF POLYCYCLIC AROMATIC HYDROCARBON PROPERTIES IN GALAXIES

Frédéric Galliano[1]

ABSTRACT

In the present contribution, I summarize a systematic study of *ISO* and *Spitzer* mid-IR spectra of Galactic regions and star forming galaxies. This study quantifies the relative variations of the main aromatic features inside spatially resolved objects as well as among the integrated spectra of 50 objects. Our analysis implies that the properties of the PAHs are remarkably universal throughout our sample and at different spatial scales. In addition, the relative variations of the band ratios, as large as one order of magnitude, are mainly controled by the fraction of ionized PAHs. In particular, I show that we can rule out both the modification of the PAH size distribution and the mid-IR extinction, as an explanation of these variations. High values of the $I_{6.2}/I_{11.3}$ ratio are found to be associated with the far-UV illuminated surface of PDRs, at the scale of an interstellar cloud, and associated with star formation activity, at the scale of a galaxy. Using a few well-studied Galactic regions, we provide an empirical relation between the $I_{6.2}/I_{11.3}$ ratio and the ionization/recombination ratio $G_0/n_e\sqrt{T_{\rm gas}}$. Finally, I show that these trends are consistent with the detailed modeling of the PAH emission within photodissociation regions, taking into account the radiative transfer, the stochastic heating and the charge exchange between gas and dust.

Subject headings: astrochemistry — (ISM:) dust — ISM: lines and bands — ISM: molecules — infrared: ISM, galaxies

1. INTRODUCTION

Polycyclic Aromatic Hydrocarbons (PAHs) are large molecules containing ∼10 to 1000 carbon atoms. They are commonly believed to be the carriers of the ubiquitous broad mid-infrared features, centered around 3.3, 6.2, 7.7, 8.6 and 11.3 μm (e.g. Allamandola et al.

[1]Department of Astronomy, University of Maryland, College Park, MD 20742 (galliano@astro.umd.edu)

1999). Due to their small size, these molecules are predomantly excited by single UV-photon events. At solar metallicity, $\sim 15\%$ of the total infrared (IR) luminosity is radiated through the aromatic features (e.g. Zubko et al. 2004). On the contrary, PAHs are underabundant in low-metalicity environments (Galliano et al. 2008a, for a complete study).

It has long been surmised that the mid-infrared emission features provide a clear signature of the interaction of far-UV photons with cloud surfaces and hence a probe of the importance of massive star formation in a region (Genzel et al. 1998; Peeters et al. 2004). The present work extends this by studying methodically the mid-infrared spectra of a wide variety of sources at different spatial scales, and investigating the physical origin of the PAH band ratio variations.

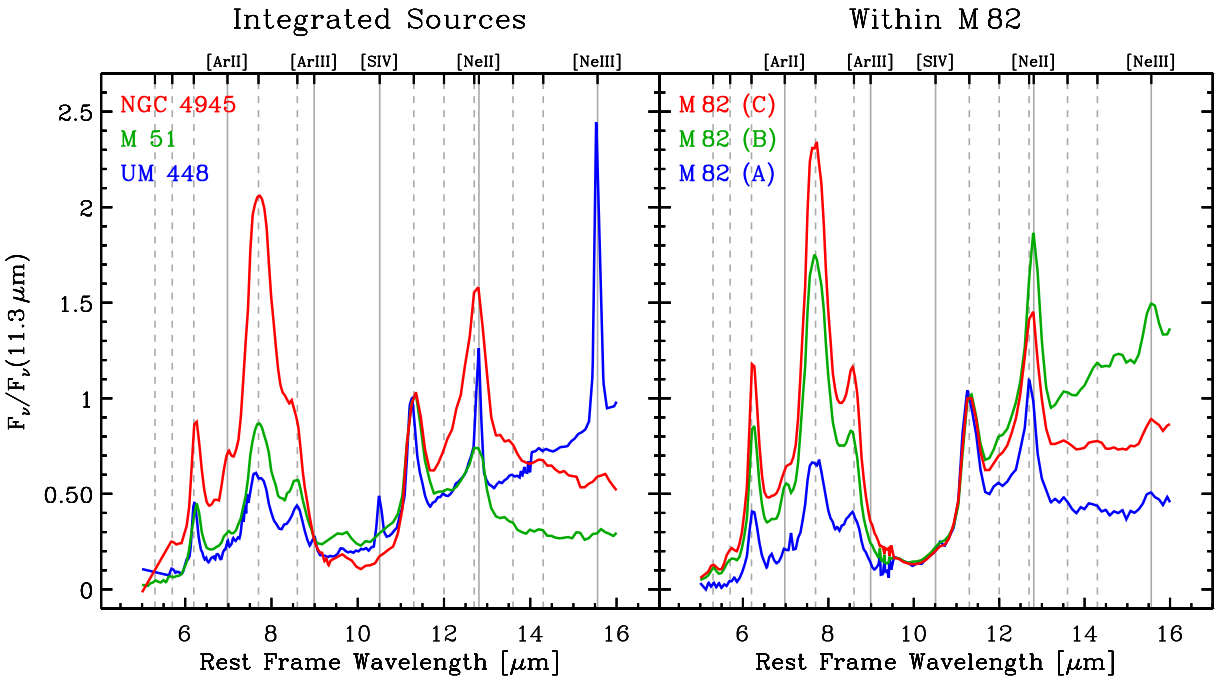

Fig. 1.— *Qualitative demonstration of the aromatic feature variations in galaxies (Galliano et al. 2008b). Both panels show mid-infrared spectra normalised by the monochromatic flux in the 11.3 μm feature.* Left panel: *integrated spectra of three galaxies; a blue compact dwarf, UM 448; a spiral M 51; a ULIRG NGC 4945.* Right panel: *spatially resolved spectra in three different regions in the starburst galaxy M 82; (A) is in the halo; (B) is at an end of the disc; (C) is in the starburst region.*

2. SYSTEMATIC ANALYSIS OF THE OBSERVED AROMATIC FEATURES

2.1. Sample and Mid-Infrared Spectral Decomposition

We have constructed a large sample of mid-infrared spectra of Galactic regions (H II regions, photodissociation regions, planetary nebulae), Magellanic H II regions, and nearby dwarf, spiral and starburst galaxies. These sources were observed with one of the three following instruments: *ISO*/CAM, *ISO*/SWS, *Spitzer*/IRS. Several of these objects have been spectrally mapped (IC 342, M 17, M 51, M 82, M 83, 30 Doradus, and the Orion bar). Our sources are the merging of the samples presented by Madden et al. (2006) and Galliano et al. (2008a). They present a wide range of properties (metallicity, star formation rates), as well as of spatial scales (resolution of ~ 0.1 pc in M 17 and the Orion bar, and of ~ 0.1 kpc in external galaxies). Fig. 1 illustrates the diversity of these properties.

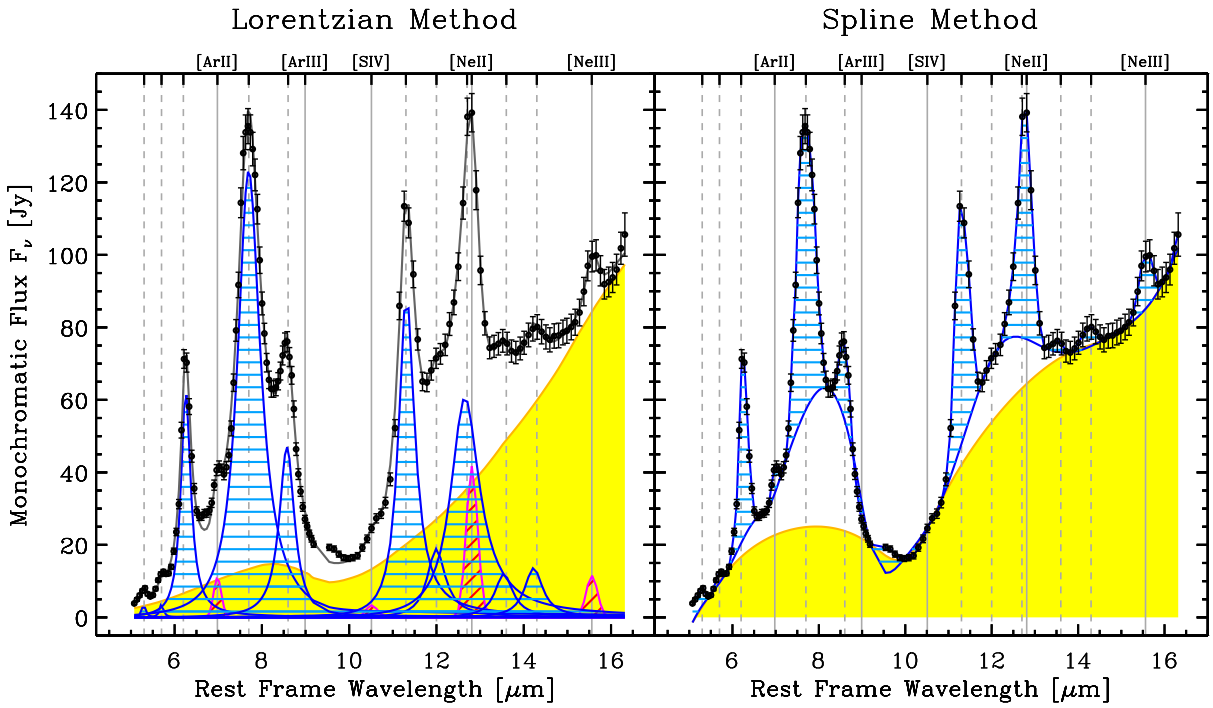

Fig. 2.— *Demonstration of the two methods used to decompose all our mid-IR spectra, on the spectrum of M 82 (Galliano et al. 2008b).* Left panel: *the continuum (yellow filled) is the sum of two modified blackbodies; the aromatic features (blue shaded) are Lorentz profiles; the ionic lines (pink shaded) are gaussian functions.* Right panel: *the continuum (yellow filled) is a spline function; the plateaus under the bands (empty areas) are also spline functions; the aromatic bands and ionic lines (blue shaded) are the residuals.*

Quantifying the spectral variations demonstrated in Fig. 1 is not straightforward. Indeed, a significant fraction of the power radiated through the aromatic features comes from their wings. Moreover the accurate profile of the bands is uncertain, and has been modeled differently by Boulanger et al. (1998), Li & Draine (2001) and Vermeij et al. (2002). In order to test the robustness of our results, we have systematically analysed our spectra using two different methods (Fig. 2). These methods are described in detail by Galliano et al. (2008b). It is important to note that the *Lorentzian method* (left panel of Fig. 2) fits Lorentz profiles to the aromatic features, taking into account the flux in their wings. This method is feature-biased, since part of the small grain continuum can artificially be accounted by the wings of the bands. On the contrary, the *Spline method* (right panel of Fig. 2), which integrates only the tip of the aromatic bands, is continuum-biased.

Although the numerical values of the intensity of a given feature, measured with the two methods are different, our study shows that the order between several intensities is identical with the two methods. It indicates that the respective biases of the methods do not affect the general trends between band intensities. Therefore, in the following of this review, I will present only the results obtained with the first method and refer the reader to Galliano et al. (2008b) for the complete results.

2.2. Correlations Between Aromatic Feature Intensity Ratios

Fig. 3 shows the correlations between several aromatic feature intensity ratios derived from integrated spectra of galaxies and Galactic regions (left panels), as well as from spatially resolved spectra within M 82 (right panels). These figures clearly show that all types of sources and all types of apertures follow the same universal trends. The 6.2, 7.7 and 8.6 μm features appear to be tied together, while the ratios between these features and the 11.3 μm band vary by one order of magnitude. The relations involving the 8.6 μm feature exhibit a larger dispersion, as this band is the weakest of the four considered here, its intensity is significantly affected by the silicate extinction feature, and it is blended with the powerful 7.7 μm feature. A preliminary version of these correlations was presented by Galliano (2004).

In general, high values of $I_{7.7}/I_{11.3}$ are associated with intense star forming regions. Fig. 4 shows images of several spectral components of the edge-on Galactic photodissociation region (PDR) M 17. On each image, the H II region is located toward the top-left corner, and the molecular cloud toward the bottom-right corner. The edge-on view of this region allows us to see the different strata of species, as demonstrated by the top left panel of Fig. 4. This panel shows that the Ne III ions are distributed on a ridge located closer to the H II region than the Ne II ions. The top right panel shows that the Ne III and the very small grain intensity have

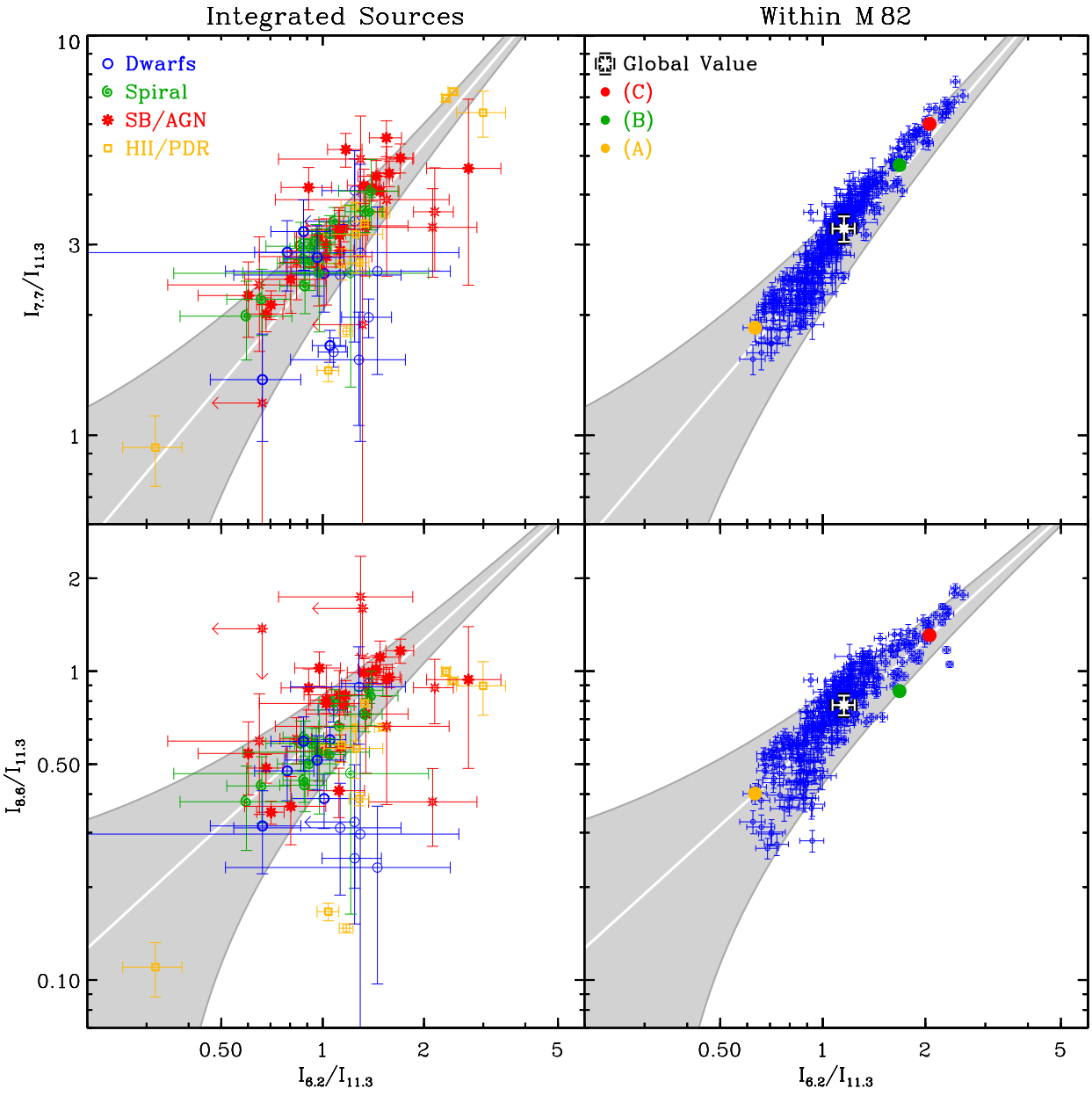

Fig. 3.— *Correlations between select aromatic feature ratios (Galliano et al. 2008b).* I_λ *refers to the intensity of the band centered around* λ μm. *Left panels: the symbols correspond to the band ratios derived from spectra integrated over an entire source; the faint symbols are fits that we consider uncertain, due either to a low signal-to-noise ratio or to a weak feature-to-continuum ratio. Right panels: the symbols correspond to the band ratios derived from spectra of individual pixels within M 82; the three regions (A, B, C) are the ones shown in Fig. 1. In all panels, the grey stripe is the linear correlation to the observations* $\pm 1 \times \sigma$.

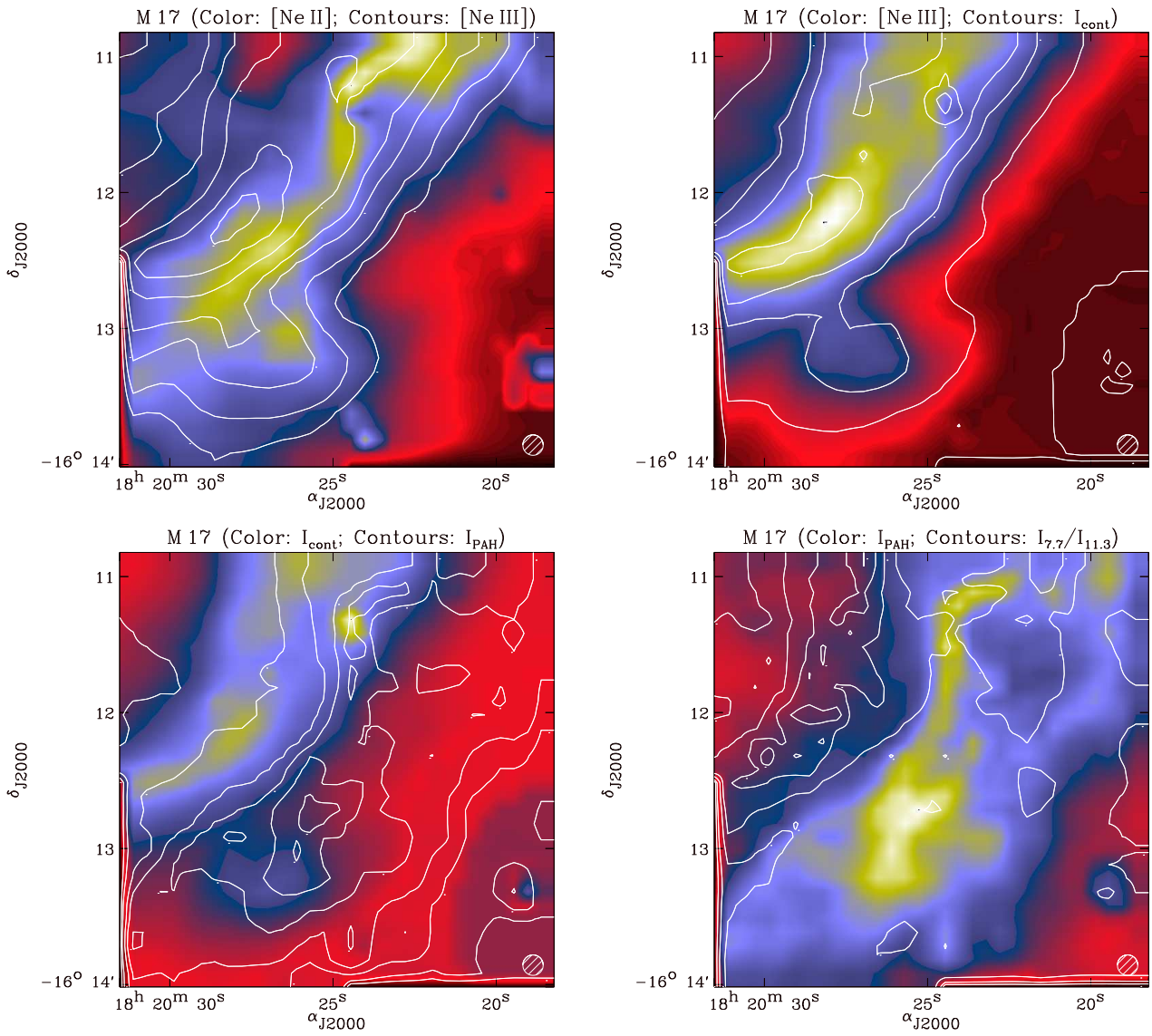

Fig. 4.— *Spatial distribution of the various mid-IR components within the Galactic PDR M 17 (Cesarsky et al. 1996; Galliano et al. 2008b). Each image compares two spectral components; the intensity increases from dark red to light yellow for the color images; the contour levels are 5, 10, 20, 30, 50, 70 and 90% of the peak intensity. The displayed components are the intensities of the* $[\mathrm{Ne\,II}]_{12.81\mu m}$ *and* $[\mathrm{Ne\,III}]_{15.56\mu m}$ *lines, of the continuum* (I_{cont}, *integrated between 10 and 16* μm), *of all the PAH bands* I_{PAH}, *and the* $\mathrm{I}_{7.7}/\mathrm{I}_{11.3}$ *ratio. The shaded circle in the bottom right corner of each figure is the beam size.*

similar spatial distributions, while the bottom left panel shows that the PAHs are found more deeply inside the cloud, since they undergo photolysis/thermolysis close to the H II region. Finally, the bottom right panel shows that the $I_{7.7}/I_{11.3}$ ratio peaks in the region where the $[Ne\,III]_{15.56\mu m}$ and the continuum intensity I_{cont} are maximum. Consequently, at the scale of an interstellar cloud, the $I_{7.7}/I_{11.3}$ ratio is maximum at the surface of the far-UV illuminated surface.

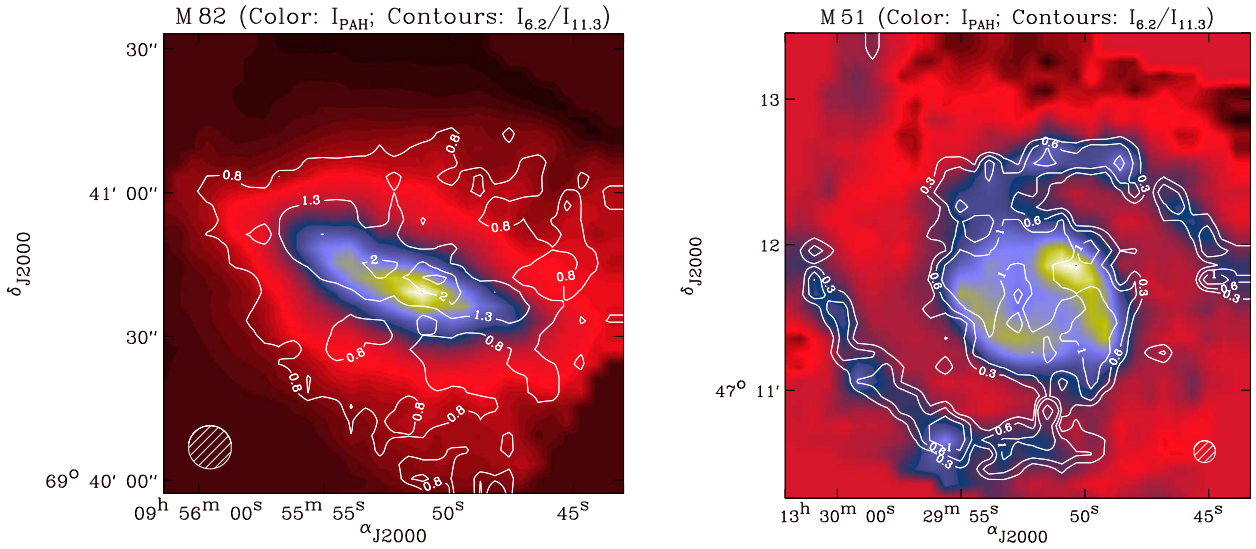

Fig. 5.— *Spatial distribution of the aromatic features in M 82 (left panel) and M 51 (right panel), from Galliano et al. (2008b). The color images show the intensity of all PAH bands (increasing from dark red to light yellow). The contours show the values of the* $I_{6.2}/I_{11.3}$ *ratio. The shaded circle is the beam size.*

Fig. 5 compares the spatial distributions of the intensity radiated by the aromatic bands to the $I_{6.2}/I_{11.3}$ ratio (following the same trends than $I_{7.7}/I_{11.3}$), within two external galaxies, M 82 and M 51. Contrary to Fig. 4, the clouds are not resolved in this case. These images indicate that the $I_{6.2}/I_{11.3}$ ratio is enhanced where the PAH intensity is high, along the spiral arms and in the starburst regions. Therefore, at the scale of a galaxy, the $I_{6.2}/I_{11.3}$ ratio is maximum in massive star forming regions.

3. ORIGIN OF THE AROMATIC FEATURE VARIATIONS IN GALAXIES

3.1. Inventory of the Physical Processes Potentially Affecting the Band Ratios

PAHs are stochastically heated, hence their thermal emission spectrum is determined by their temperature distribution. Fig. 6 demonstrates the effects of changing this temperature

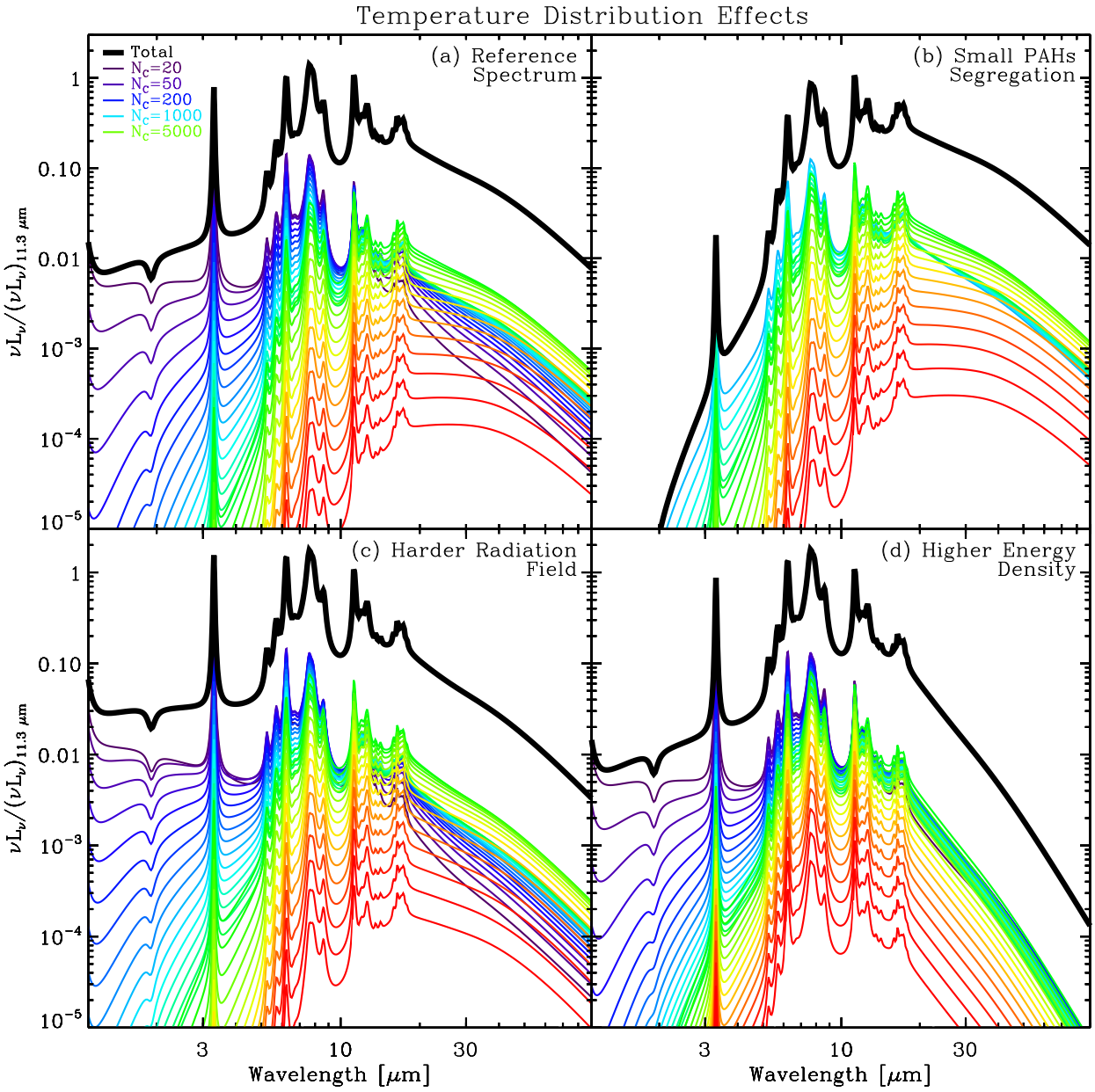

Fig. 6.— *Demonstration of the effects on the aromatic bands of changing the PAH temperature distribution. Each panel shows the theoretical spectrum of a collection of PAHs of various sizes N_C (number of carbon atoms; different colors). The total spectrum integrated over the size distribution is the black thick line. Top-left panel: we adopt the Zubko et al. (2004) size distribution, and the Galactic diffuse interstellar radiation field (ISRF; Mathis et al. 1983); this case serves as reference for the other panels. Top-right panel: the size distribution is truncated; we exclude grains smaller than $N_C = 1000$. Bottom-left panel: the ISRF is harder (instantaneous burst of 0 Myr). Bottom-right panel: the ISRF intensity is $\chi_{ISRF} = 10^5$ times higher. The absorption efficiencies are a mixture of 50% neutral and 50% ionized PAHs, from Draine & Li (2007).*

distribution by varying different parameters. Fig. 6a corresponds to the Galactic diffuse ISM. Fig. 6b shows that the bands around 6.2, 7.7 and 8.6 μm decrease relative to the 11.3 μm band, if the small PAHs (smaller than $N_{\rm C} = 1000$ carbon atoms) disappear. Indeed, small PAHs fluctuate up to higher temperatures than larger ones. Hence, their short wavelength features emit more intensely. This case corresponds to environments where the small PAHs would photosublimate preferentially. Fig. 6c shows that by increasing the hardness of the interstellar radiation field (ISRF) or equivalently by increasing the average stellar photon energy, PAHs fluctuate up to higher temperatures, therefore boosting the short wavelength features. Finally, Fig. 6d shows that increasing the radiation density decreases the time that a given PAH spend on average at cool temperatures. However, this effect plays a role only for ISRFs which are $\chi_{\rm ISRF} \gtrsim 10^5$ times more intense than the Galactic one.

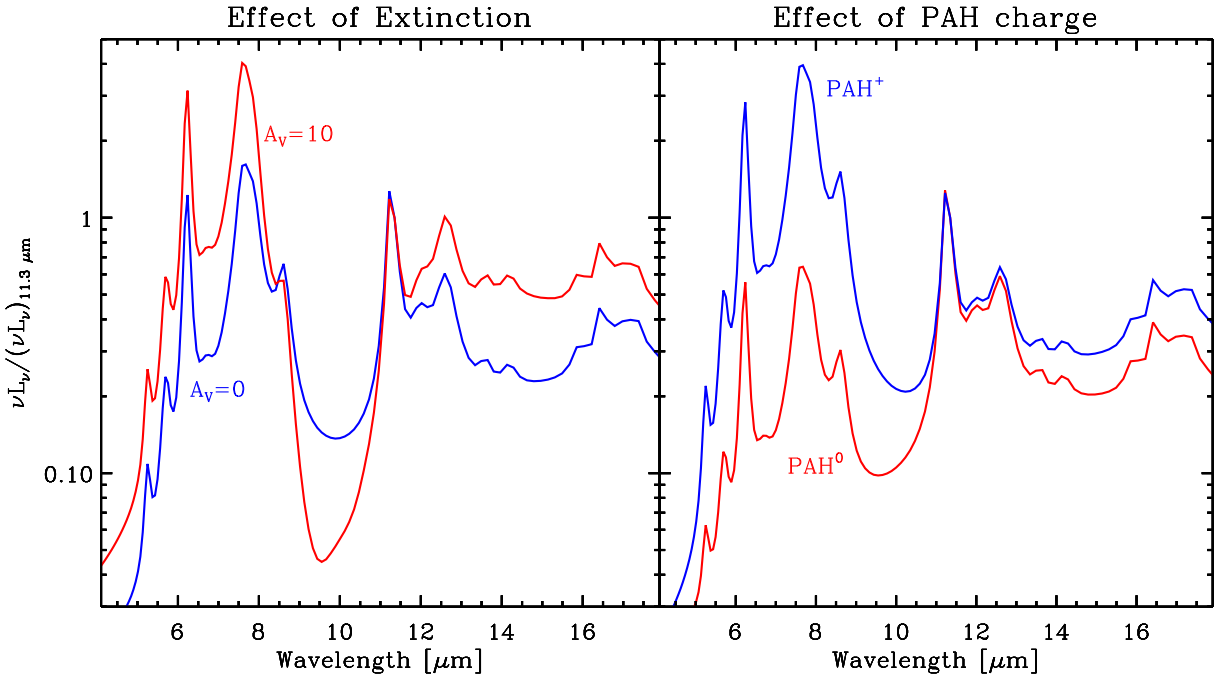

Fig. 7.— *Demonstration of the effects on the aromatic bands of the extinction and of the charge of the PAHs. Both panels show the theoretical spectra with the Zubko et al. (2004) size distribution, the Draine & Li (2007) absorption efficiencies, irradiated by the Mathis et al. (1983) ISRF. Left panel: the reference spectrum (blue) is compared to the same spectrum extincted by a screen with an $A_V = 10$ (red). Right panel: the red and blue spectra correspond to neutral and ionized PAHs.*

Fig. 7 demonstrates additional effects controling the aromatic feature ratios. First, mid-IR extinction is dominated by a broad silicate feature centered around 9.7 μm. This feature absorbs significantly the 8.6 μm and 11.3 μm bands, but has little effect on the 6.2 and 7.7 μm bands, as shown on the left panel of Fig. 7. Second, the 6 to 9 μm features are

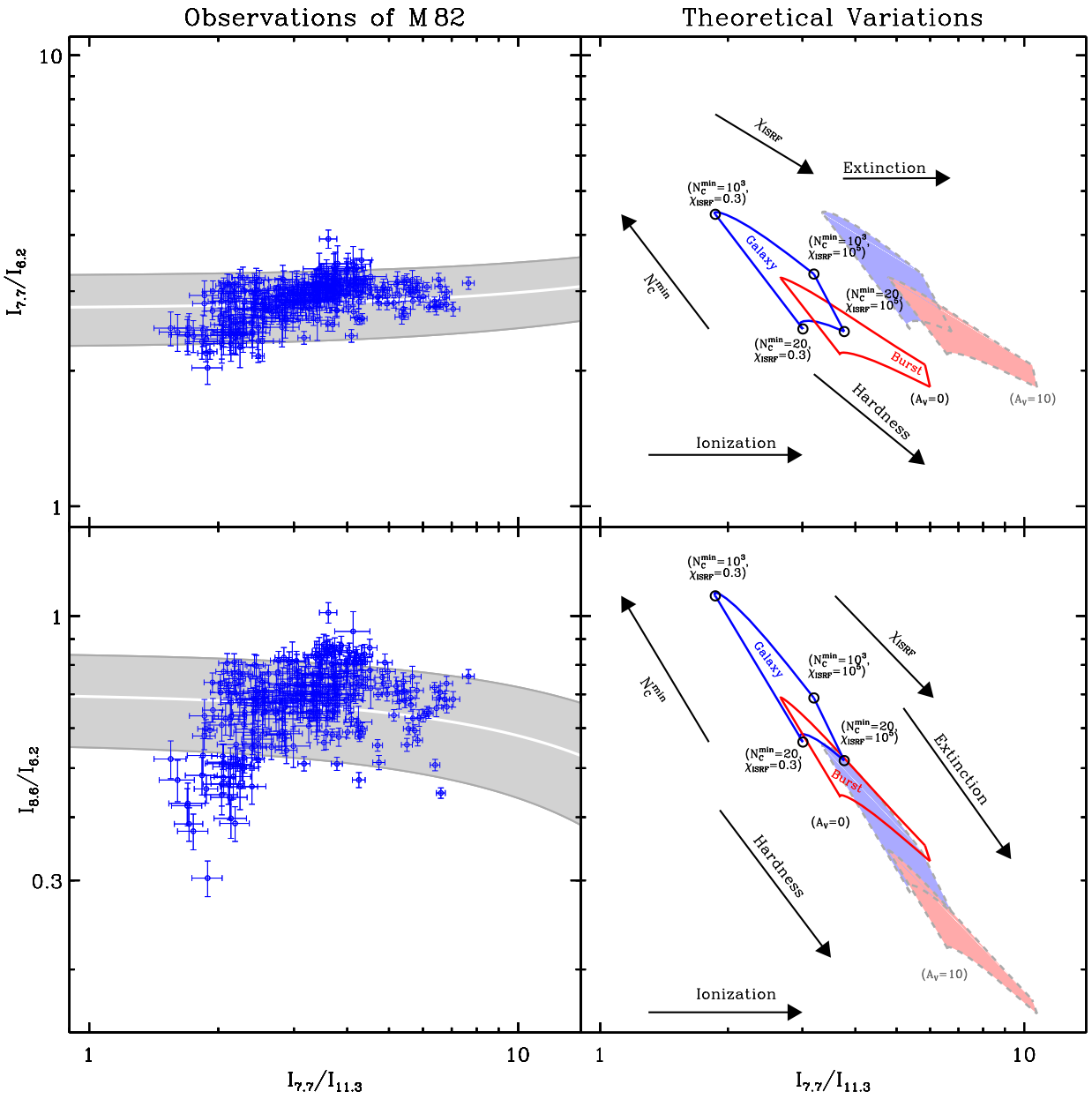

Fig. 8.— *Comparison between observed and theoretical trends of aromatic feature intensity ratios. Left panels: observed correlations within M 82 (right panels of Fig. 3); the grey stripes are line fits $\pm 1 \times \sigma$ to the observations. Right panels: presentation of the results of the modeling shown in Figs. 6-7. In each panel, the blue empty polygon with the circled corners shows the effect of varying both the minimum cut-off PAH size, N_C^{min}, and the ISRF intensity, χ_{ISRF}, with the Galactic ISRF (labeled Galaxy). The values between parenthesis, close to each corners are the values of these two parameters at the corner. Second, the red empty polygon is the analog of the previous one, except that the ISRF is now a harder one (labeled Burst). Finally, the two filled polygons are the analogs of the two previous ones, except that we applied a screen extinction with $A_V = 10$. The various arrows show the sense of variation of the band ratios with each parameter.*

enhanced for charged PAHs (right panel of Fig. 7), since they are attributed to C-C modes, while the 11.3 μm is attributed to peripheral C-H modes (e.g. Allamandola et al. 1989).

3.2. The Dominant Role of the Fraction of Ionized PAHs

Fig. 8 compares the trend between band ratios observed within M 82 (similar trends are followed by the other sources; Fig. 3) to theoretical trends. The left panels of Fig. 8 are another way to look at Fig. 3. Statistically, the observed $I_{7.7}/I_{6.2}$ and $I_{8.6}/I_{6.2}$ do not show significant variations and are uncorrelated with the $I_{7.7}/I_{11.3}$. The right panels of Fig. 8 represents the variations of the aromatic features from the models presented in Figs. 6-7. What this figure shows is that the modification of the PAH temperature distribution (Sect. 3.1) is not consistent with our observations, since it would anticorrelate $I_{7.7}/I_{6.2}$ and $I_{8.6}/I_{6.2}$ with $I_{7.7}/I_{11.3}$. On the other hand, the extinction produces the right trend between $I_{7.7}/I_{6.2}$ and $I_{7.7}/I_{11.3}$, but it anticorrelates $I_{8.6}/I_{6.2}$ with $I_{7.7}/I_{11.3}$. Finally, Fig. 8 shows that the only effect which is consistent with the observations is the variation of the fraction of ionized PAHs.

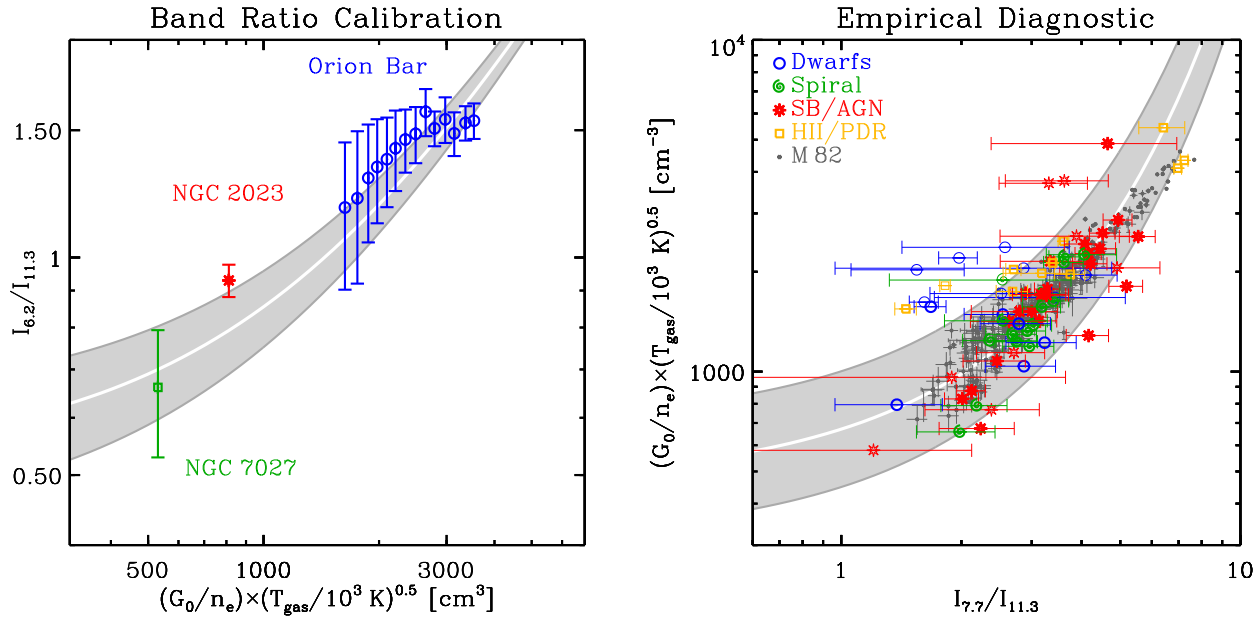

Fig. 9.— *Empirical relation between the aromatic feature intensity ratio and the ionization-to-recombination ratio. Left panel: calibration of the band ratio, using well calibrated sources; the values of G_0, n_e and T_{gas} come from detailed PDR modeling. Right panel: inversion of the right panel relation; the sources shown are the ones from Fig. 3. The grey stripe is the line fit $\pm 1 \times \sigma$.*

We emphasize that our sample contains mainly moderately obscured star forming galaxies and Galactic regions, where AGNs are under-represented. The effects that have been ruled out here may play a role for peculiar sources like elliptical galaxies (Kaneda et al. 2007), LINERs (Smith et al. 2007) or ULIRGs (Brandl et al. 2006).

4. THE AROMATIC BANDS AS A DIAGNOSTIC TOOL OF THE PHYSICAL CONDITIONS

4.1. Empirical Calibration of the Mid-Infrared Band Ratios

The variations of aromatic feature intensity ratios are mainly controled by the fraction of charged PAHs (Sect. 3.2). This fraction of charged PAHs is directly related to the ionization-to-recombination ratio, $G_0/n_e\sqrt{T_{\rm gas}}$, where G_0 is the UV field density, n_e is the electron density, and $T_{\rm gas}$ is the gas temperature. Therefore the observed aromatic feature intensities can provide useful constraints on the physical conditions in the region where they are emitting.

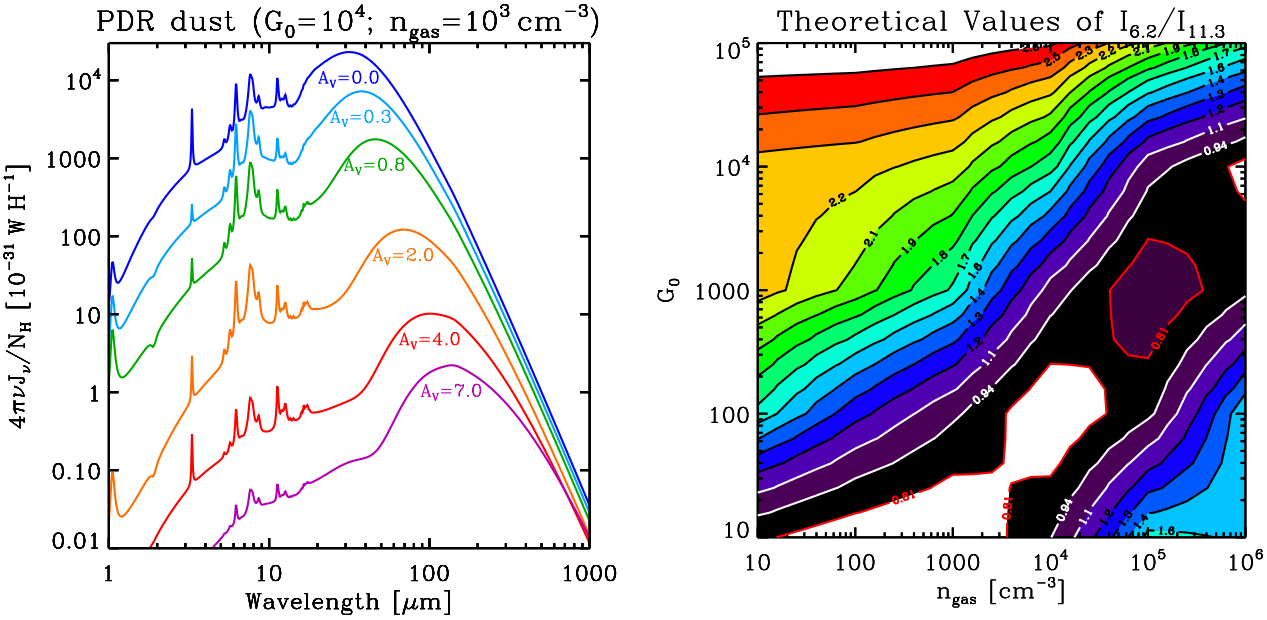

Fig. 10.— *PAH and PDR self-consistent modeling, taking into account the radiative transfer, PAH stochastic heating and charge exchange between gas and dust (Galliano et al. 2008c). Left panel: SEDs at different locations (corresponding to different attenuations A_V) within a given slab PDR having a density of $n_{gas} = 10^3$ cm^{-3} and incident UV field of $G_0 = 10^4$ in Habing units. Right panel: theoretical aromatic feature ratio diagram; each (G_0, n_e) coordinate corresponds to a single face-on integrated PDR.*

We used the G_0, n_e and $T_{\rm gas}$ values from the literature of a few well-studied sources, in order to provide an empirical calibration of the band ratio (Galliano et al. 2008b). The left panel of Fig. 9 shows this calibration. It demonstrates that the $I_{6.2}/I_{11.3}$ ratio (or the relative fraction of PAH^+) is high for either high G_0 (proportional to the ionization rate) or low $n_e/\sqrt{T_{\rm gas}}$ (proportional to the recombination rate). This calibration can be applied to the sources in Fig. 3 (right panel of Fig. 9).

4.2. Detailed PDR Modeling of the Polycylic Aromatic Hydrocarbon Emission

The empirical relation of Fig. 9 can be generalised theoretically, using detailed PDR modeling. The left panel of Fig. 10 shows the dust spectral energy distributions (SEDs) at different points within an homogeneous slab PDR. The radiative transfer of the incident ISRF on the surface of the cloud is solved, in combination with the photoionization, photodissociation and chemical reactions within the cloud, using the PDR model of Kaufman et al. (2006). In particular, this PDR model takes into account the charge transfer between gas and dust, and thus determines the fraction of charged PAHs at each point within the cloud. Using the Draine & Li (2007) absorption efficiencies, we solved the stochastic heating of the PAHs and small grains for each $A_{\rm V}$ (left panel of Fig. 10; Galliano et al. 2008c).

The right panel of Fig. 10 shows the value of the PAH band ratio integrated over each PDR of UV field G_0 and density n_e. This type of diagram is usual for PDR gas lines. The originality of this work is to extend it to dust features. This figure is in qualitative agreement with Fig. 9. It shows that the $I_{6.2}/I_{11.3}$ ratio is constant over constant G_0/n_e lines. The $I_{6.2}/I_{11.3}$ is high at the top-left corner of the panel, for high G_0 and low n_e, where the PAHs are mainly positively charged. The $I_{6.2}/I_{11.3}$ is also high at the botton-right corner of the panel, for low G_0 and high n_e, since the PAHs are mainly negatively charged.

The present study has developed the observed mid-IR features as a quantitative tool to probe the physical conditions (e.g. $G_0/n_e \times \sqrt{T_{\rm gas}}$) in the emitting regions. We expect that this study will be of fundamental value for the interpretation of *Spitzer* data as well as future *Sofia* and *JWST* observations of galaxies in the nearby and early universe.

REFERENCES

Allamandola, L. J., Hudgins, D. M., & Sandford, S. A. 1999, ApJ, 511, L115

Allamandola, L. J., Tielens, G. G. M., & Barker, J. R. 1989, ApJS, 71, 733

Boulanger, F., Boisssel, P., Cesarsky, D., & Ryter, C. 1998, A&A, 339, 194

Brandl, B. R., Bernard-Salas, J., Spoon, H. W. W., et al. 2006, ApJ, 653, 1129

Cesarsky, D., Lequeux, J., Abergel, A., et al. 1996, A&A, 315, L305

Draine, B. T. & Li, A. 2007, ApJ, 657, 810

Galliano, F. 2004, PhD thesis, University of Paris XI

Galliano, F., Dwek, E., & Chanial, P. 2008a, ApJ, 672, 214

Galliano, F., Madden, S. C., Tielens, A. G. G. M., Peeters, E., & Jones, A. P. 2008b, ApJ accepted, astro-ph/0801.4955

Galliano, F., Wolfire, M. G., Tielens, A. G. G. M., et al. 2008c, ApJ, in prep.

Genzel, R., Lutz, D., Sturm, E., et al. 1998, ApJ, 498, 579

Kaneda, H., Onaka, T., & Sakon, I. 2007, ApJ, 666, L21

Kaufman, M. J., Wolfire, M. G., & Hollenbach, D. J. 2006, ApJ, 644, 283

Li, A. & Draine, B. T. 2001, ApJ, 554, 778

Madden, S. C., Galliano, F., Jones, A. P., & Sauvage, M. 2006, A&A, 446, 877

Mathis, J. S., Mezger, P. G., & Panagia, N. 1983, A&A, 128, 212

Peeters, E., Spoon, H. W. W., & Tielens, A. G. G. M. 2004, ApJ, 613, 986

Smith, J. D. T., Draine, B. T., Dale, D. A., et al. 2007, ApJ, 656, 770

Vermeij, R., Peeters, E., Tielens, A. G. G. M., & van der Hulst, J. M. 2002, A&A, 382, 1042

Zubko, V., Dwek, E., & Arendt, R. G. 2004, ApJS, 152, 211